Thermal Decomposition of Silver Carbonate: Phenomenology and Physico-geometrical Kinetics

Nobuyoshi Koga,*[,†] Shuto Yamada,[‡] and Tomoyasu Kimura[†]

[†]Chemistry Laboratory, Graduate School of Education, Hiroshima University, 1-1-1 Kagamiyama, Higashi-Hiroshima 739-8524, Japan
[‡]Faculty of Arts and Science, Kyusyu University, 744 Motooka, Fukuoka 819-0395, Japan

Supporting Information

1. Characterization of samples

Typical XRD patterns and FT-IR spectra of the samples listed in Table 1 are shown in Figs. S1 and S2, respectively. No distinguishable difference was found among the XRD patterns of the different samples, and all the XRD peaks observed were assigned to those of the RT phase of Ag_2CO_3 (monoclinic, S.G.=$P2_1/m$, a=4.8521, b=9.5489, c=3.2536 Å, β=91.9713 º).[S1]

All the major IR absorption bands are identical among the different samples, and agree with those reported previously.[S2-4] The broad absorption band around 1300-1500 cm^{-1} corresponds to the ν_3 mode of the carbonate ion. The ν_1 and ν_2 modes of the carbonate ion appear at 1070 and 802 cm^{-1}, respectively. The splitting absorption peaks at 721 and 705 cm^{-1} are attributed to the ν_4 mode of the carbonate ion. The peak at 1786 cm^{-1} has been described as the $\nu_1+\nu_4$ modes of the carbonate ion.

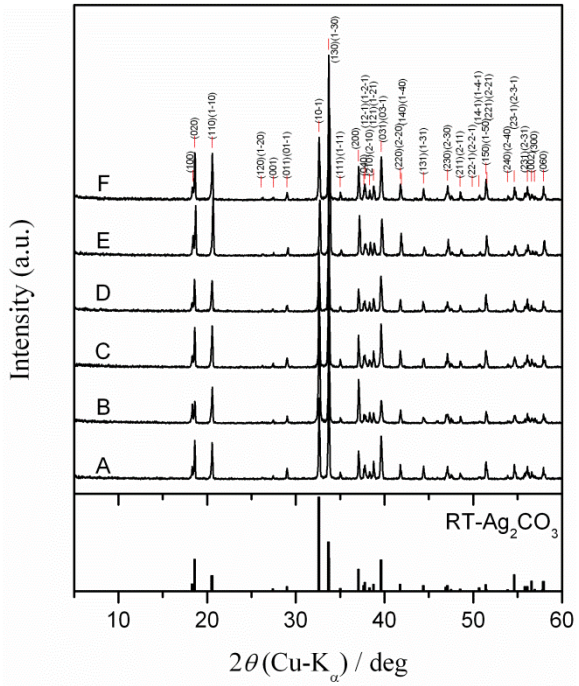

Figure S1. The XRD patterns of the samples, together with the XRD pattern of the RT phase of Ag_2CO_3 simulated from the reported crystallographic data.[S1]

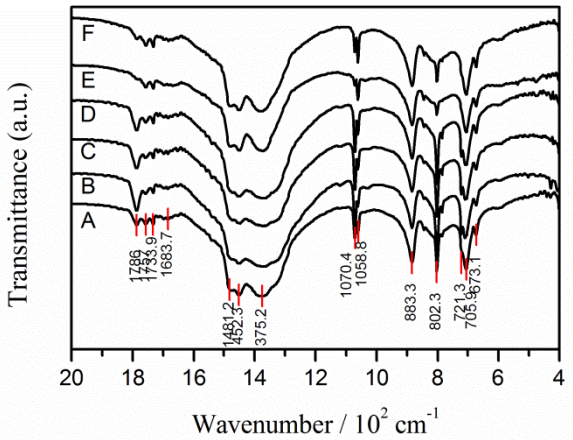

Figure S2. The FT-IR spectra of the samples.

2. Changes in the crystalline phases during heating in flowing N_2

Figure S3 compares the changes in the XRD patterns of sample A during heating under different heating programs. On heating the sample under the stepwise isothermal heating program, Fig. S3(a), the thermal decomposition of Ag_2CO_3 to Ag_2O occurs at 448-498 K. The product phase of the reaction is preferentially single phase Ag_2O, in view of XRD. Thermal decomposition of the intermediate product to Ag is observed in the temperature range of 598-648 K. Under linearly increasing temperature at β=5 K min^{-1}, Fig. S3(b), the solid product of the reaction at 448-498 K is a mixed phase of Ag_2O and the high temperature phase of Ag_2CO_3, α-Ag_2CO_3 (hexagonal, S.G.=*P*-62*m*, *a*=9.0924, *b*=9.0924, *c*=3.3249 Å) [S1] as shown in Fig. S4. The intermediate mixed phase is stable up to 598 K until it thermally decomposes to Ag.

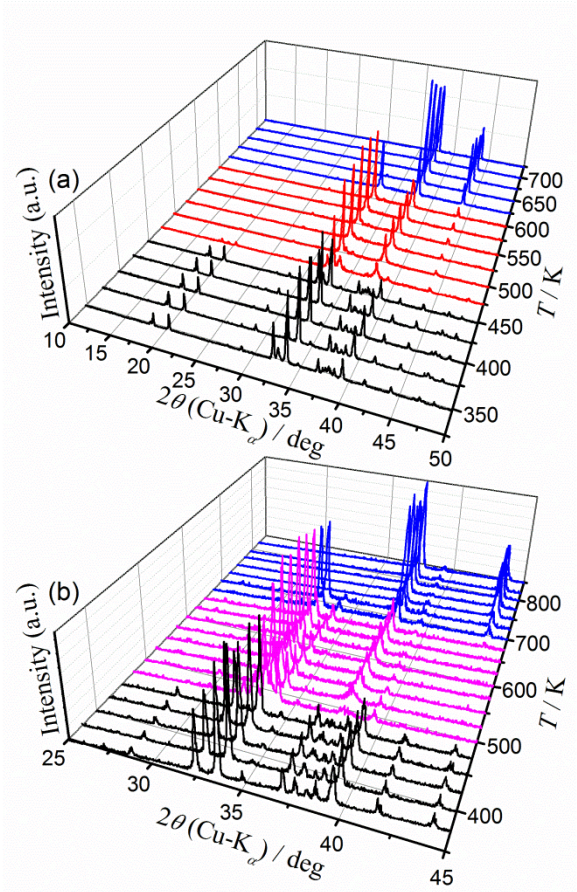

Figure S3. Changes in the XRD pattern during heating sample A in flowing N_2 (100 cm^3 min^{-1}): (a) stepwise isothermal heating and (b) linear nonisothermal heating at β=5 K min^{-1}.

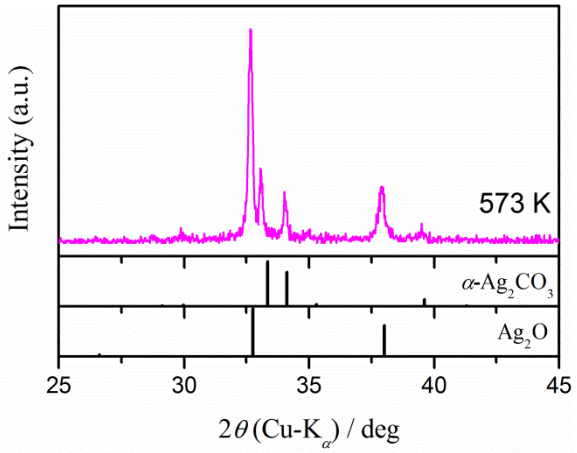

Figure S4. Typical XRD pattern of sample A heated linearly to 573 K at β=5 K min^{-1} in flowing N_2 (100 cm^3 min^{-1}), together with the XRD patterns of α-Ag_2CO_3 and Ag_2O simulated from the reported crystallographic data.[S1]

3. Thermal behavior in flowing CO_2

Figure S5 compares the TG-DTA curves of thermal decomposition of sample A in flowing N_2 and CO_2. In flowing CO_2, the first mass-loss step shifts to higher temperature as expected from the chemical equilibrium of the reaction: $Ag_2CO_3 \rightleftarrows Ag_2O + CO_2$. In flowing CO_2, two endothermic peaks appear in the temperature region of the first mass-loss step in flowing N_2. The mass-loss fraction of the first mass-loss step does not change practically in flowing N_2 and CO_2. This indicates that the atmospheric CO_2 does not influence the arrest of reaction (1). The second mass-loss step practically starts at the same temperature in flowing N_2 and CO_2. Because the second mass-loss step of the arrested sample starts after being triggered by reaction (2) as was observed from the mass-chromatograms of the evolved gases, the initiation temperature of the second mass-loss step is not influenced by atmospheric CO_2.

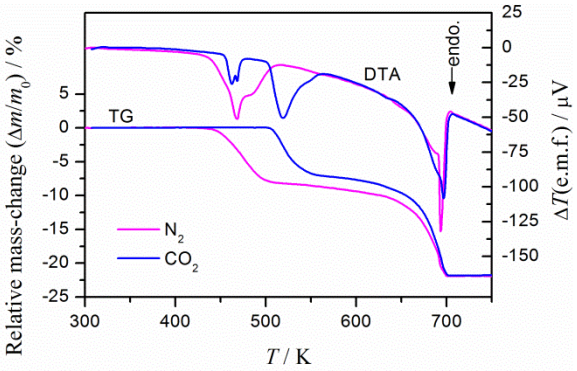

Figure S5. Comparisons of the TG-DTA curves, in flowing N_2 (80 cm^3 min^{-1}) and in flowing CO_2 (80 cm^3 min^{-1}), for sample A (m_0=15.0 mg) at β=5 K min^{-1}.

4. Structural phase transitions in Ag_2CO_3

Table S1 summarizes the transition temperatures and the enthalpy changes of the structural phase transitions of Ag_2CO_3 in samples A-C during the cyclical heating/cooling runs as shown in Fig. 6. In view of the total ΔH of the RT→β→α transitions observed in the first heating run, the values are nearly identical among the samples, where the detectable difference in the ΔH values is possible because of the partial decomposition to Ag_2O as well as the possible impurities because a larger value is observed for the less active sample in thermal decomposition. The most distinguishable difference of the phase transition behavior among the samples can be seen in the transition temperature of RT→β. If the transition temperature of RT→β depends on the grain size, assumed to explain the large shift of the transition temperature to lower temperature by repeated heating, the difference in the transition temperature among the samples indicate the different grain size of the RT phases produced by the transition of β→RT.

Table S1. Transition temperatures and enthalpy changes in the structural phase transitions of Ag_2CO_3 in samples A-C.

Sample	Transition	Run	$T_{e.o.}$ / K	T_p / K	ΔH / kJ mol^{-1}
A (type III)	RT→β	1st heating	456.7±0.9	464.4±0.4	-----
	RT→β→α	1st heating	-----	-----	5.45±0.05
	RT→β	3rd heating	446.7±0.8	453.7±0.4	3.51±0.03
	β→α	2nd heating	469.3±0.5	-----	1.94±0.02
	α→β	1st cooling	459.8±0.4	-----	–2.05±0.03
	β→RT	2nd cooling	385.8±0.3	-----	–2.65±0.05
B (type I)	RT→β	1st heating	451.5±0.3	458.4±0.3	-----
	RT→β→α	1st heating	-----	-----	5.36±0.08
	RT→β	3rd heating	432.5±0.4	443.1±0.4	3.56±0.06
	β→α	2nd heating	467.1±0.3	-----	1.80±0.03
	α→β	1st cooling	460.2±0.3	-----	–1.88±0.07
	β→RT	2nd cooling	383.7±0.6	-----	–2.41±0.01
C (type II)	RT→β	1st heating	452.8±0.3	459.5±0.3	-----
	RT→β→α	1st heating	-----	-----	5.57±0.06
	RT→β	3rd heating	442.5±0.4	450.9±0.3	3.58±0.04
	β→α	2nd heating	468.0±0.3	-----	1.98±0.03
	α→β	1st cooling	460.1±0.2	-----	–2.07±0.03
	β→RT	2nd cooling	392.3±0.2	-----	–2.83±0.05

5. Formal kinetic analysis of the first mass-loss step

The kinetic rate data recorded under isothermal and constant rate conditions were analyzed simultaneously by assuming the following differential kinetic equation for the ideal single reaction step.[S5-8]

$$\frac{d\alpha}{dt} = A\exp\left(-\frac{E_a}{RT}\right) f(\alpha) \qquad \text{(S1)}$$

where α, A, and E_a are the fractional reaction, the Arrhenius preexponential factor, and the apparent activation energy, respectively. The kinetic model function $f(\alpha)$ expresses the physico-geometry of the reaction.

Figure S6 illustrates the results of the formal kinetic analysis for thermal decomposition of sample A. Taking the logarithms of eq.(S1), we obtain[S9,10]

$$\ln\left(\frac{d\alpha}{dt}\right) = \ln\left[Af(\alpha)\right] - \frac{E_a}{RT} \qquad \text{(S2)}$$

According to eq.(S2), the data points of the respective kinetic rate data at a selected α should create a straight line on the plot of $\ln(d\alpha/dt)$ against T^{-1}. The isoconversional plots, known as the Friedman plot,[S9] at different α from 0.1 to 0.9 in steps of 0.1 are shown in Fig. S6(a). Regardless of the data points under isothermal and constant mass-loss rate conditions, the data points ($\ln(d\alpha/dt)$, T^{-1}) at the restricted α form a line. However, the slope of the Friedman plots, $-E_a/R$, change depending on α. The α-dependent change of E_a evaluated from the slopes of the Friedman plots are shown in Fig. S6(b). Because constant E_a during the course of the reaction is a prerequisite for Eq. (S1), the observed variation in E_a indicates the possibility of a multi-step reaction.

As an approximate procedure, an experimental master plot of the overall process was drawn, using the average value of E_a = 96.3 ± 1.0 kJ mol^{-1} in the range $0.1 \le \alpha \le 0.9$, by calculating the hypothetical reaction rate by extrapolating the kinetic rate data to infinite temperature, $d\alpha/d\theta$, at different α.[S7,8,10]

$$\frac{d\alpha}{d\theta} = \frac{d\alpha}{dt}\exp\left(\frac{E_a}{RT}\right)$$

$$\text{with} \qquad \theta = \int_0^t \exp\left(-\frac{E_a}{RT}\right) dt \qquad \text{(S3)}$$

where θ is Ozawa's generalized time[S11] and denotes the hypothetical reaction time extrapolated to infinite temperature. Figure S6(c) shows the experimental master plot of $(d\alpha/d\theta)$ against α. The experimental master plot indicates the deceleration in the concave shape during the first-half of the reaction, which subsequently switches to convex shape. For the well-defined single step reaction, the experimental master plot is correlated to A and $f(\alpha)$ by[S7,8,10]

$$\frac{d\alpha}{d\theta} = Af(\alpha) \qquad \text{(S4)}$$

However, the experimental master plot in Fig. S6(c) cannot be described by any single physico-geometrical reaction models typically used for solid-state reactions. Using an empirical kinetic model known as the Sestak-Berggern model,[S12] SB(m,n,p): $f(\alpha)=\alpha^m(1-\alpha)^n[-\ln(1-\alpha)]^p$, the experimental master plot is fitted by SB(−1.20±0.70,0.50±0.26,0.79±0.68) with A=(1.63±0.09)×10^7 s^{-1}.

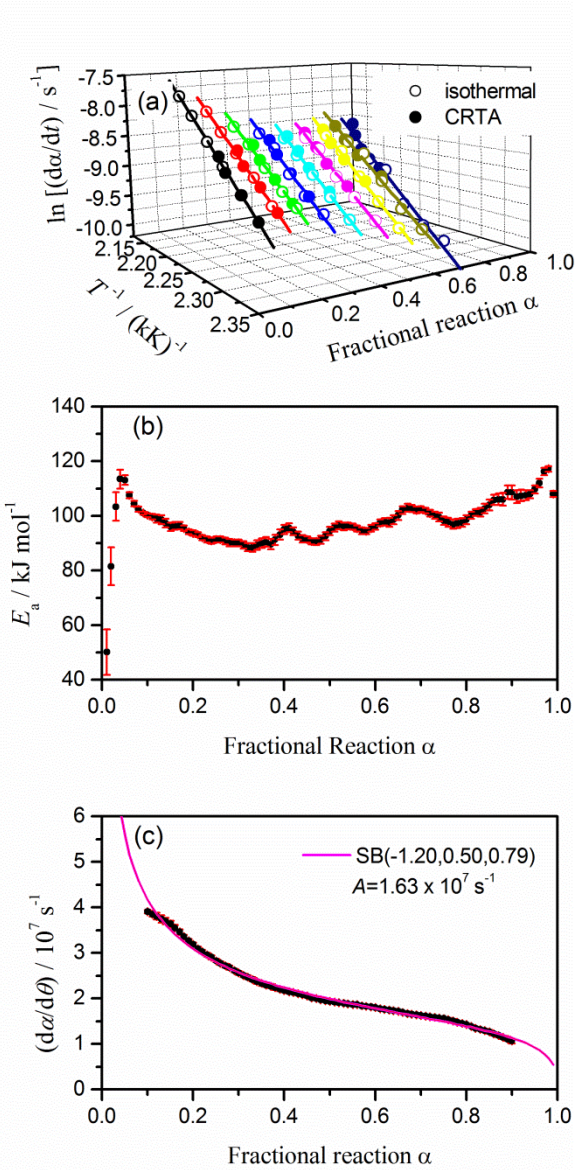

Figure S6. Kinetic results for thermal decomposition of sample A from Ag_2CO_3 to Ag_2O under isothermal and controlled rate conditions in flowing N_2 (80 cm^3 min^{-1}). (a) The Friedman plots at different α from 0.1 to 0.9 in steps of 0.1, (b) the values of E_a at different α, and (c) the experimental master plot and the fitted curve using the SB(m, n, p) model.

6. Mathematical deconvolution of the first mass-loss step

For the quick estimation of the extent of the contribution of the component reaction stages in the multi-stage thermal decomposition of Ag_2CO_3 to Ag_2O, the derivative mass-loss curves recorded at different constant temperatures were deconvoluted using the PeakFit Ver.4.2 software. The Weibull function, eq.(S5), was employed for the estimation due to the satisfactory fitting of the reported overlapping multi-step reactions in the solid-state.[S13]

$$y = a_0\left(\frac{a_3-1}{a_3}\right)^{\frac{1-a_3}{a_3}}\left(\frac{x-a_1}{a_2}+\left(\frac{a_3-1}{a_3}\right)^{\frac{1}{a_3}}\right)^{a_3-1}\exp\left[-\left(\frac{x-a_1}{a_2}+\left(\frac{a_3-1}{a_3}\right)^{\frac{1}{a_3}}\right)^{a_3}+\frac{a_3-1}{a_3}\right] \quad \text{(S5)}$$

where a_0~a_3 are the amplitude, center, width, and shape, respectively.

Figure S7 compares the typical results of the mathematical deconvolution for thermal decomposition of Ag_2CO_3 to Ag_2O of samples B and C. The average values of the mass-loss fractions of the different reaction stages calculated for the derivative mass-loss curves at different temperatures are listed in Table S2. The mass-loss fractions of the different reaction stages are largely different between the samples B and C. The mass-loss fractions are first estimated and they are subsequently utilized as the default values of the optimization parameters in the kinetic deconvolution described in the main body of the article.

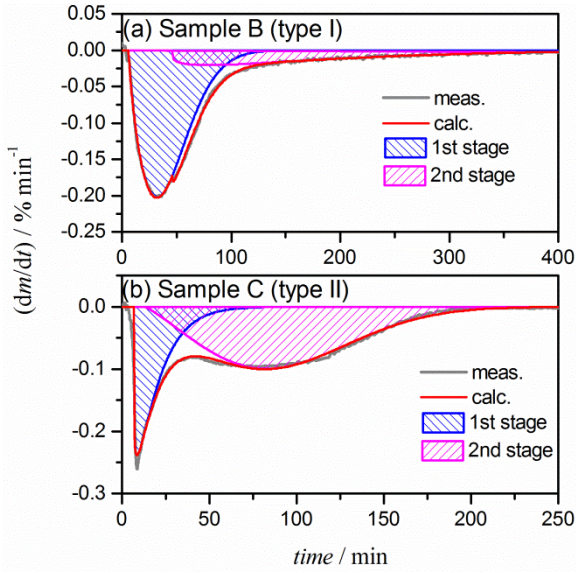

Figure S7. Typical results of the mathematical deconvolution using the Weibull function for the derivative mass-loss data, recorded isothermally at 453 K, for thermal decomposition of Ag_2CO_3 to Ag_2O.

Table S2. The mass-loss fractions of the first and second reaction stages evaluated by the mathematical deconvolution of the derivative mass-loss curves at constant temperatures

Sample	1st reaction stage	2nd reaction stage
B (type I)	0.77 ± 0.04	0.23 ± 0.04
C (type II)	0.27 ± 0.04	0.73 ± 0.04

References for Supporting Information

(S1) Norby, P.; Dinnebier, R.; Fitch, A. N. *Inorg. Chem.* **2002**, *41*, 3628-3637.
(S2) Ross, S. D.; Goldsmith, J. *Spectrochim. Acta* **1964**, *20*, 781-784.
(S3) Allen, J.; Scaife, P. *Aus. J. Chem.* **1966**, *19*, 715-724.
(S4) Zehnder, E.-J. *J. Mol. Struct.* **1983**, *98*, 49-53.
(S5) Málek, J. *Thermochim. Acta* **1992**, *200*, 257-269.
(S6) Koga, N.; Tanaka, H. *J. Therm. Anal.* **1993**, *40*, 1173-1179.
(S7) Koga, N. *Thermochim. Acta* **1995**, *258*, 145-159.
(S8) Gotor, F. J.; Criado, J. M.; Malek, J.; Koga, N. *J. Phys. Chem. A* **2000**, *104*, 10777-10782.
(S9) Friedman, H. L. *J. Polym. Sci. C* **1964**, *6*, 183-195.
(S10) Ozawa, T. *J. Therm. Anal.* **1986**, *31*, 547-551.
(S11) Ozawa, T. *Bull. Chem. Soc. Jpn.* **1965**, *38*, 1881-1886.
(S12) Sestak, J.; Berggren, G. *Thermochim. Acta* **1971**, *3*, 1-12.
(S13) Perejon, A.; Sanchez-Jimenez, P. E.; Criado, J. M.; Perez-Maqueda, L. A. *J. Phys. Chem. B* **2011**, *115*, 1780-1791.